Density functional theory study of hydrophobic zeolites for the removal of triclosan from aqueous solution

Michael Fischer

Crystallography & Geomaterials Research, Faculty of Geosciences, University of Bremen, Klagenfurter Straße 2-4, 28359 Bremen, Germany

Bremen Center for Computational Materials Science and MAPEX Center for Materials and Processes, University of Bremen, 28359 Bremen, Germany

E-Mail: michael.fischer@uni-bremen.de

SUPPORTING INFORMATION

Index

Further details of force field calculations

Force field parameters

Calculations addressing isolated TCS and the adsorption of TCS and/or H_2O in all-silica zeolites used default *pcff* parameters. Partial charges and the parameters defining the Lennard-Jones potentials used to represent long-range attraction and short-range repulsion between atoms that are not bonded to each other are given in **Table S1**. It should be noted that *pcff* uses 9-6 Lennard-Jones potentials[1] and a 6th-power combination rule.[2] In the calculations for protonated zeolites, the charge on the framework proton was modified from the default value of +0.0839 e[-] to the formal charge of +1.0 e[-]. Although this adjustment might possibly lead to an overestimation of the electrostatic contribution, it was found that the use of a higher positive charge on the framework proton was pivotal to obtain configurations in which the negatively polarised areas of the guest molecules are located in the vicinity of the framework proton, thus constituting suitable starting points for the DFT optimisations. Both Monte Carlo (MC) and molecular dynamics (MD) simulations used an atom-based summation for Lennard-Jones potentials, employing a cutoff distance of 12.5 Å with a cubic spline truncation. Ewald summation (MD simulations) and a combination of Ewald summation and group-based summation (MC simulations) were used for electrostatic interactions.

Monte Carlo simulations

Monte Carlo (MC) simulations were carried out using the Materials Studio (MS) *Sorption* module. The calculations were done for fixed sorbate loading at T = 298 K, setting the loading to 1 TCS molecule or 8 H_2O molecules per simulation cell (see main text). While the H_2O molecule and the zeolite frameworks were treated as rigid entities, rotations about the three C−O bonds were included as torsional degrees of freedom. In configurational-bias MC simulations of TCS adsorption, the probability ratio of different MC moves corresponded to 3:2:1:1:1 for exchange (insertion/deletion), regrowth, intramolecular torsion, molecule translation, and molecule rotation, respectively. For H_2O adsorption simulations, the probability ratio in the Metropolis sampling was 2:0.1:1:1 for exchange, regrowth, translation, and rotation. For each zeolite-guest combination, three independent simulations were run, and five low-energy snapshots were extracted manually.

Molecular dynamics simulations

Both the MD-based simulated annealing runs to obtain starting structures for the DFT optimisations and the MD simulations of TCS diffusion used the MS *Forcite* module. Typical simulated annealing runs consisted of 20 annealing cycles, with each cycle consisting of 200,000 simulation steps (timestep 0.5 fs). All framework atoms were held fixed in these calculations. For protonated zeolites, the position of the O atom of the guest molecule closest to the framework proton was also constrained to avoid a breaking of the hydrogen bond during the simulated annealing. In order to sample different degrees of freedom of the TCS molecule, simulations of TCS@Zeo systems used an initial temperature of 300 K and a mid-cycle temperature of 1000 K. Since the use of such a high mid-cycle temperature was found to break

clusters of H_2O molecules, simulated annealing runs involving water used a starting temperature of 298 K and a mid-cycle temperature of 373 K. The simulations used a Nosé thermostat with a Q ratio of 0.01. The configurations obtained at the end of each cycle were optimised, and five low-energy configurations were extracted manually from the total set of 100 configurations (5 simulated annealing runs with 20 cycles each).

MD simulations of TCS diffusion through all-silica zeolites were carried out for a temperature of 298 K, sampling a total duration of 50 ns using a timestep of 0.5 fs. In these simulations, the zeolite frameworks were treated as fully flexible. These simulations, which started from the low-energy configurations obtained in the simulated annealing runs, also used a Nosé thermostat with a Q ratio of 0.01. Self-diffusion coefficients were computed from the mean square displacements of TCS using the Einstein relation.
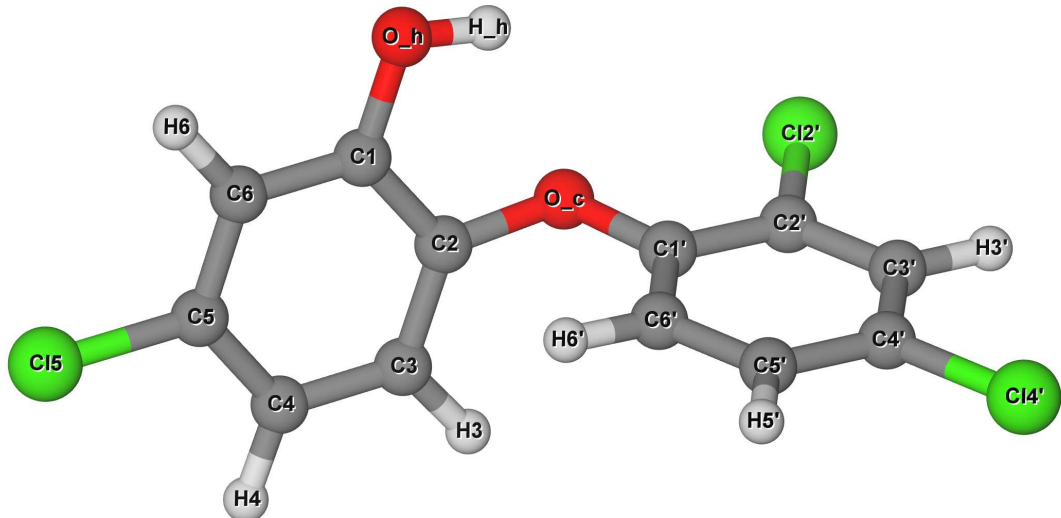

Figure S1: TCS molecule with atom labels used in **Table S1**. Labels are consistent with the crystal structure reported by Ramos et al.,[3] with the exception of the hydroxyl group and the central oxygen atom, which were relabelled in the present work.

Parameters of force field calculations

Table S1: Atom types and non-bonded *pcff* parameters used in force field calculations. TCS atom labels correspond to those displayed in **Figure S1**. Partial charges q and Lennard-Jones parameters R_0 and D_0 are given for each atom.

TCS molecule	Atom type (*pcff*)	q [e$^-$]	R_0 [Å]	D_0 [kcal mol^{-1}]
O_c	oc	−0.0530	3.530	0.2400
O_h	oh	−0.4506	3.530	0.2400
H_h	ho	0.4241	1.098	0.0130
C1, C2, C1'	cp	0.0265	4.010	0.0640
C3, C4, C6, C3', C5', C6'	cp	−0.1268	4.010	0.0640
C5, C2', C4'	cp	0.1020	4.010	0.0640
Cl5, Cl2', Cl4'	cl	−0.1020	3.920	0.2247
H3, H4, H6, H3', H5', H6'	hc	0.1268	2.995	0.0200
H₂O molecule				
O	o*	-0.7982	3.608	0.2740
H	hw	0.3991	1.098	0.0130
Zeolite				
Si	sz	0.5236[a]	[b]	[b]
Al	az	0.5366[a]	[b]	[b]
O, Si−O−Si	oss	-0.2618[a]	3.4506	0.1622
O, Si−O−Al, no proton	oas	-0.2959[a]	5.2591	0.0129
O, Si−O−Al, protonated	ob	-0.2515[a]	5.2191	0.0135
H	hb	+1.0000	1.2149	5.2302

a) In H-FAU and H-MOR, charges on framework Si, Al, O atoms are slightly changed from the tabulated values to compensate the customised charge of +1 on the framework proton.

b) Si and Al are treated as non-interacting except for electrostatic interactions.

Cell parameters of DFT-optimized zeolite structures

Table S2: Cell parameters of DFT-optimized zeolite structures. Cell multiplications used in setting up the supercells for guest@Zeo configurations are also included. References given in the last column correspond to publications from which the starting structures for the optimizations were taken.

FTC	Symmetry	a [Å]	b [Å]	c [Å]	α [°]	β [°]	γ [°]	Supercell	Ref.
AFI	$P3_1$	13.671	13.671	8.328	90	90	120	a)	4
IFR	$C2/m$[b)]	18.629	13.496	7.631	90	78.38	90	1×2×3	5
MOR	$Cmc2_1$	18.061	20.209	7.455	90	90	90	1×1×3	6
BEA	$P4_122$	12.470	12.470	26.331	90	90	90	2×2×1	7
FAU	$Fd\bar{3}m$	24.258	24.258	24.258	90	90	90	1×1×1	8
CFI	$P1$	13.695	5.021	25.497	90	90	90	2×4×1	9
H-FAU	$P1$	24.258	24.258	24.258	90	90	90	1×1×1	8
H-MOR	$P1$	18.061	20.209	22.364	90	90	120	1×1×1	6

a) An orthogonal supercell was constructed using the following transformations:

$$\vec{a}_{ortho} = 2 \cdot \vec{a}_{hex} + \vec{b}_{hex} \qquad \vec{b}_{ortho} = \vec{b}_{hex} \qquad \vec{c}_{ortho} = 3 \cdot \vec{c}_{hex}$$

b) Changed cell setting with respect to original publication

Comparison of proton positions in H-FAU

Table S3: Total energies and relative energies with respect to lowest-energy model for H-FAU models with the proton bonded to different O atoms. The last column indicates whether the proton is accessible to guest molecules.

Proton location	E_{total} [Ha]	E_{rel} [kJ mol⁻¹]	Accessible?
H@O1	-6947.10406	5.4	Yes (pointing into 12MR)
H@O2	-6947.10611	0	No (pointing into 6MR connecting *sod* and *d6r* cage)
H@O3	-6947.10204	10.7	Yes (pointing into 6MR bordering the FAU supercage)
H@O4	-6947.10137	12.4	Yes (pointing into 12MR)

# Comparison of Al sites and proton positions in H-MOR
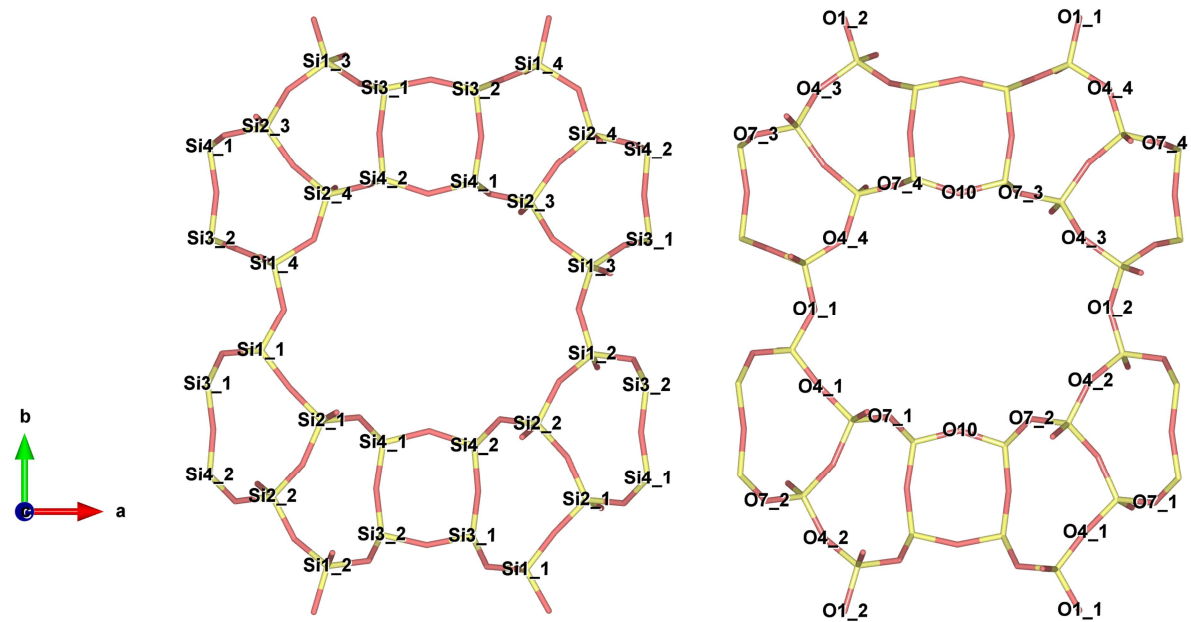
Figure S2: Surroundings of one 12MR channel in all-silica MOR (symmetry: $P2_12_12_1$) including labels of Si atoms (left panel) and O atoms (right panel). Only those O atoms that constitute the channel wall are labeled.

Table S4: Total energies and relative energies with respect to lowest-energy model for different H-MOR models. Different Al sites and proton positions were considered, limiting the choice to those cases where the proton is located at the wall of the 12MR channel.

Al site	Proton location	E_{total} [Ha]	E_{rel} [kJ mol^{-1}]
Al@T1_1	H@O1_1	-5210.15911	7.8
Al@T1_1	H@O4_1	-5210.15251	25.1
Al@T1_2	H@O1_2	-5210.15531	17.8
Al@T1_2	H@O4_2	-5210.15823	10.1
Al@T1_3	H@O1_2	-5210.15720	12.8
Al@T1_3	H@O4_3	-5210.15993	5.7
Al@T1_4	H@O1_1	-5210.15896	8.2
Al@T1_4	H@O4_4	-5210.16208	0
Al@T2_1	H@O4_1	-5210.15690	13.6
Al@T2_1	H@O7_1	-5210.16012	5.2
Al@T2_2	H@O4_2	-5210.15644	14.8
Al@T2_2	H@O7_2	-5210.15930	7.3
Al@T2_3	H@O4_3	-5210.15633	15.1
Al@T2_3	H@O7_3	-5210.15763	11.7
Al@T2_4	H@O4_4	-5210.15987	5.8
Al@T2_4	H@O7_4	-5210.15819	10.2
Al@T4_1	H@O7_1	-5210.15718	12.9
Al@T4_1	H@O7_3	-5210.15972	6.2
Al@T4_1	H@O10	-5210.15554	17.2
Al@T4_2	H@O7_2	-5210.15673	14.1
Al@T4_2	H@O7_4	-5210.15819	10.2
Al@T4_2	H@O10	-5210.15624	15.4

Adsorption energies from DFT optimisations

Table S5: Adsorption energies ΔE_{ads} and deformation energies calculated for TCS@Zeo complexes (all values in kJ mol^{-1}). For each configuration, adsorption energies obtained with DZVP-MOLOPT-SR basis sets and with TZVP-MOLOPT basis sets are included. Lowest-energy configurations (TZVP) are highlighted in bold.

	ΔE_{ads} (DZVP-SR)	ΔE_{ads} (TZVP)	$\Delta E_{deform,Zeo}$ (TZVP)	$\Delta E_{deform,TCS}$ (TZVP)
BEA, Config1	**-179.2**	**-156.2**	**1.8**	**2.6**
BEA, Config2	-179.7	-155.5	1.7	1.2
BEA, Config3	-161.7	-132.6	1.6	9.1
BEA, Config4	-169.8	-146.0	1.5	2.5
BEA, Config5	-152.5	-126.5	1.6	11.2
FAU, Config1	-146.8	-120.3	2.1	3.7
FAU, Config2	-144.9	-120.4	3.2	1.5
FAU, Config3	**-149.5**	**-124.1**	**2.7**	**1.4**
FAU, Config4	-132.0	-105.5	2.8	13.4
FAU, Config5	-130.4	-106.2	2.8	3.4
AFI, Config1	**-181.3**	**-156.2**	**1.5**	**1.6**
AFI, Config2	-179.9	-154.5	1.5	2.5
AFI, Config3	-176.4	-149.0	2.2	3.3
AFI, Config4	-167.2	-138.7	1.1	17.4
AFI, Config5	-161.9	-131.0	1.0	17.8
IFR, Config1	**-190.4**	**-160.4**	**3.7**	**3.0**
IFR, Config2	-190.9	-159.7	4.7	3.1
IFR, Config3	-173.7	-143.7	2.4	5.1
IFR, Config4	-181.4	-150.1	4.8	4.2
IFR, Config5	-181.9	-151.6	4.0	5.9
MOR, Config1	-183.8	-151.4	4.7	5.9
MOR, Config2	-182.4	-153.3	1.8	5.3
MOR, Config3	-187.2	-154.6	4.9	4.8
MOR, Config4	**-185.5**	**-155.3**	**5.4**	**4.6**
MOR, Config5	-171.6	-139.2	4.0	23.2
CFI, Config1	**-193.5**	**-153.8**	**1.7**	**2.0**
CFI, Config2	-199.7	-151.6	4.9	2.1
CFI, Config3	-180.1	-152.2	2.6	2.5
CFI, Config4	-180.2	-134.2	4.3	16.1
CFI, Config5	-178.8	-134.7	3.3	16.6
H-FAU, Config1	-156.2	-129.5	12.5	26.0
H-FAU, Config2	-173.4	-140.7	19.6	23.4
H-FAU, Config3	-158.3	-133.7	14.3	21.9
H-FAU, Config4	**-182.5**	**-153.7**	**19.5**	**5.5**
H-FAU, Config5	-166.3	-142.5	10.7	9.3
H-MOR, Config1	-217.0	-181.7	14.9	23.0
H-MOR, Config2	**-222.9**	**-191.4**	**11.1**	**12.6**
H-MOR, Config3	-217.9	-187.4	15.0	12.7
H-MOR, Config4	-201.2	-171.1	9.7	17.0
H-MOR, Config5	-191.7	-160.3	9.0	32.2

Table S6: Adsorption energies ΔE_{ads}, zeolite deformation energies and guest-guest interaction energies calculated for 8H$_2$O@Zeo complexes (all values in kJ mol^{-1}). Adsorption energies obtained with DZVP-MOLOPT-SR basis sets and with TZVP-MOLOPT basis sets are given for the whole (H$_2$O)$_8$ cluster and per H$_2$O molecule. Lowest-energy configurations (TZVP) are highlighted in bold. For H-FAU and H-MOR, the proton transfer from the framework to the H$_2$O cluster precludes a meaningful calculation of the deformation energies.

	ΔE_{ads} 8/1 H$_2$O (DZVP-SR)	ΔE_{ads} 8/1 H$_2$O (TZVP)	$\Delta E_{deform,Zeo}$ (TZVP)	$\Delta E_{guest-guest,H2O}$ (TZVP)
FAU, Config1	**-406.7 / -50.8**	**-390.5 / -48.8**	**5.4**	**-287.6**
FAU, Config2	-407.7 / -51.0	-389.2 / -48.7	6.2	-298.8
FAU, Config3	-407.6 / -51.0	-388.6 / -48.6	6.1	-286.5
FAU, Config4	-406.1 / -50.8	-388.5 / -48.6	5.0	-279.5
FAU, Config5	-405.9 / -50.7	-389.1 / -48.6	5.6	-278.4
MOR, Config1	**-452.7 / -56.6**	**-427.5 / -53.4**	**7.2**	**-291.1**
MOR, Config2	-439.1 / -54.9	-417.0 / -52.1	6.0	-293.7
MOR, Config3	-445.1 / -55.6	-419.8 / -52.5	8.5	-293.3
MOR, Config4	-438.7 / -54.8	-419.3 / -52.4	4.8	-288.7
MOR, Config5	-436.8 / -54.6	-417.2 / -52.1	5.5	-282.0
H-FAU, Config1	-499.7 / -62.5	-464.8 / -58.1		
H-FAU, Config2	**-511.1 / -63.9**	**-479.1 / -59.9**		
H-FAU, Config3	-507.5 / -63.4	-473.5 / -59.2		
H-FAU, Config4	-496.5 / -62.1	-466.5 / -58.3		
H-FAU, Config5	-479.6 / -60.0	-447.7 / -56.0		
H-MOR, Config1	-519.5 / -64.9	-484.8 / -60.6		
H-MOR, Config2	**-525.8 / -65.7**	**-494.7 / -61.8**		
H-MOR, Config3	-527.3 / -65.9	-491.3 / -61.4		
H-MOR, Config4	-515.8 / -64.5	-484.0 / -60.5		
H-MOR, Config5	-510.0 / -63.7	-477.4 / -59.7		

Table S7: Adsorption energies ΔE_{ads} calculated for NH_2O @Zeo complexes with $N = 1, 4, 12$. Results obtained with DZVP-MOLOPT-SR basis sets and with TZVP-MOLOPT basis sets are given (all values in kJ mol^{-1} and per H_2O molecule).

|	1 H_2O (DZVP-SR)	1 H_2O (TZVP)	4 H_2O (DZVP-SR)	4 H_2O (TZVP)	12 H_2O (DZVP-SR)	12 H_2O (TZVP)
FAU, Config1	-31.3	-24.6	-47.6	-44.6	-54.3	-52.1
FAU, Config2	-16.7	-15.0	-45.9	-43.8	-51.9	-50.2
FAU, Config3	-17.2	-15.3	-46.6	-43.1	-53.9	-51.9
FAU, Config4	-31.1	-25.8	-46.1	-43.7	-53.8	-51.4
FAU, Config5	-20.7	-16.6	-46.9	-44.0	-52.0	-49.7
MOR, Config1	-43.9	-37.5	-49.1	-46.8	-57.3	-54.9
MOR, Config2	-43.1	-38.5	-49.2	-47.1	-56.0	-53.4
MOR, Config3	-45.8	-38.4	-49.1	-46.4	-57.7	-53.6
MOR, Config4	-33.7	-24.3	-50.5	-47.3	-55.3	-52.9
MOR, Config5	-19.2	-17.6	-49.3	-47.2	-54.6	-51.4
H-FAU, Config1	-89.3	-86.1	-62.0	-57.1	-60.8	-57.7
H-FAU, Config2	-89.3	-86.2	-62.2	-58.1	-61.5	-58.1
H-FAU, Config3	-89.3	-85.5	-63.2	-58.3	-59.4	-56.3
H-FAU, Config4	-89.5	-86.0	-72.5	-68.5	-57.1	-54.0
H-FAU, Config5	-79.7	-74.4	-68.8	-64.1	-61.2	-57.5
H-MOR, Config1	-88.6	-85.2	-71.3	-66.8	-64.5	-60.2
H-MOR, Config2	-89.6	-85.1	-64.0	-62.6	-69.0	-64.6
H-MOR, Config3	-89.3	-85.9	-71.8	-67.3	-64.5	-60.4
H-MOR, Config4	-89.7	-86.6	-64.0	-60.1	-63.0	-59.4
H-MOR, Config5	-89.4	-84.5	-76.5	-71.8	-68.2	-63.7
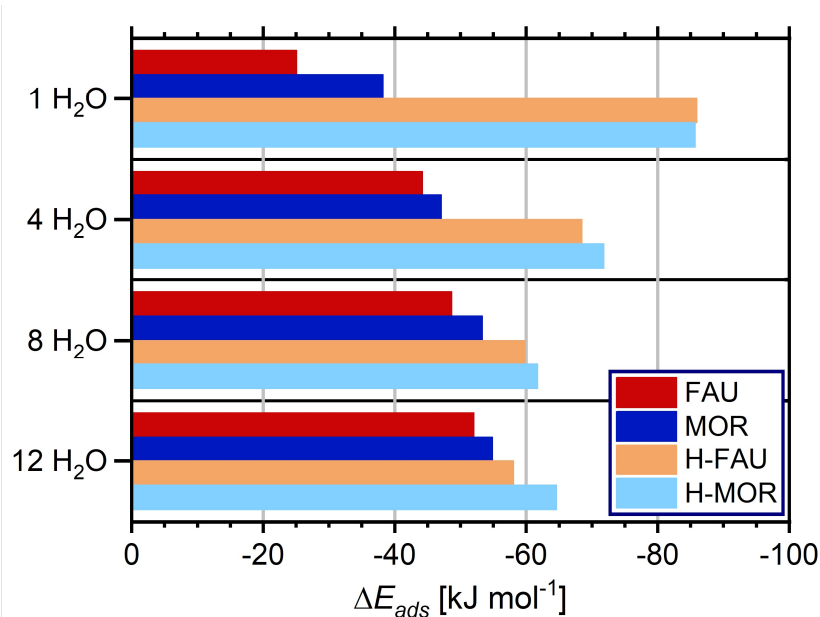
Figure S3: Boltzmann-weighted adsorption energies obtained for clusters of H_2O molecules of different size. All results are given per H_2O molecule.

Table S8: Adsorption energies ΔE_{ads} calculated for all-silica FAU and MOR with co-adsorbed TCS and water (all values in kJ mol^{-1}). As described in the main text, the label at the top indicates the order in which the species were added in the preliminary MC simulations.

	8H$_2$O@(TCS@Zeo)		TCS@(8H$_2$O@Zeo)	
	ΔE_{ads} (DZVP-SR)	ΔE_{ads} (TZVP)	ΔE_{ads} (DZVP-SR)	ΔE_{ads} (TZVP)
FAU, Config1	-574.6	-537.0	-562.6	-525.6
FAU, Config2	**-602.5**	**-558.3**	-578.1	-544.0
FAU, Config3	-569.6	-528.6	-564.4	-524.5
FAU, Config4	-595.0	-554.3	-562.4	-530.9
FAU, Config5	-564.8	-531.1	-587.5	-546.9
MOR, Config1	-644.7	-585.1	-626.6	-570.7
MOR, Config2	**-645.7**	**-591.1**	-645.8	-590.6
MOR, Config3	-618.4	-561.4	-638.4	-581.3
MOR, Config4	-636.2	-584.9	-633.6	-579.8
MOR, Config5	-624.1	-563.1	-651.3	-595.7

Additional results of AIMD simulations

Table S9: Average kinetic and potential energies from production stages of individual AIMD trajectories. The average temperature and its standard deviation are also given.

	$\bar{E}_{kin}$ [Ha]	$\bar{E}_{pot}$ [Ha]	T [K]
TCS, Traj1	0.03264	-149.46422	298.8±47.2
TCS, Traj2	0.03286	-149.46712	300.8±48.5
TCS, Traj3	0.03278	-149.46470	300.0±47.9
FAU, Traj1	0.81161	-6947.54685	297.7±10.1
FAU, Traj2	0.81086	-6947.54690	297.4±9.9
FAU, Traj3	0.81235	-6947.54549	297.9±10.1
TCS@FAU, Traj1	0.84636	-7097.05570	297.9±10.1
TCS@FAU, Traj2	0.84544	-7097.06082	297.6±9.7
TCS@FAU, Traj3	0.84631	-7097.05857	297.9±9.7
MOR, Traj1	0.60821	-5210.79884	297.8±11.6
MOR, Traj2	0.60794	-5210.80111	297.6±11.5
MOR, Traj3	0.60790	-5210.80042	297.6±11.6
TCS@MOR, Traj1	0.64283	-5360.33160	298.1±11.2
TCS@MOR, Traj2	0.64155	-5360.33281	297.5±12.1
TCS@MOR, Traj3	0.64284	-5360.32761	298.1±11.4
H-FAU, Traj1	0.81569	-6946.27213	298.6±9.8
H-FAU, Traj2	0.81522	-6946.27263	298.5±10.0
H-FAU, Traj3	0.81054	-6946.27684	296.8±9.9
TCS@H-FAU, Traj1	0.85045	-7095.79736	298.9±9.4
TCS@H-FAU, Traj2	0.84834	-7095.79923	298.1±9.8
TCS@H-FAU, Traj3	0.84653	-7095.80119	297.5±9.7
H-MOR, Traj1	0.61036	-5209.53489	298.1±11.6
H-MOR, Traj2	0.61049	-5209.53634	298.2±11.6
H-MOR, Traj3	0.60972	-5209.53790	297.8±11.8
TCS@H-MOR, Traj1	0.63987	-5359.08286	296.1±10.7
TCS@H-MOR, Traj2	0.64578	-5359.07707	298.8±11.6
TCS@H-MOR, Traj3	0.64342	-5359.08126	297.7±11.8
8H_2O@(TCS@H-FAU), Traj1	0.88091	-7233.82590	297.7±9.9
8H_2O@(TCS@H-FAU), Traj2	0.88074	-7233.81923	297.6±9.8
8H_2O@(TCS@H-FAU), Traj3	0.88150	-7233.82807	297.9±9.6
8H_2O@(TCS@H-MOR), Traj1	0.67759	-5497.12562	297.8±10.9
8H_2O@(TCS@H-MOR), Traj2	0.67980	-5497.12464	298.8±11.2
8H_2O@(TCS@H-MOR), Traj3	0.68060	-5497.12304	299.1±11.2

Table S10: Adsorption energies ΔE_{ads} computed from DFT-optimised low-energy frames of AIMD trajectories for 8H$_2$O@(TCS@Zeo) systems (all values in kJ mol^{-1}).

	ΔE_{ads} (DZVP-SR)	ΔE_{ads} (TZVP)
8H$_2$O@(TCS@H-FAU), Traj1	-654.6	-613.6
8H$_2$O@(TCS@H-FAU), Traj2	-650.0	-597.9
8H$_2$O@(TCS@H-FAU), Traj3	-667.2	-601.4
8H$_2$O@(TCS@H-MOR), Traj1	-762.8	-685.7
8H$_2$O@(TCS@H-MOR), Traj2	-751.1	-678.9
8H$_2$O@(TCS@H-MOR), Traj3	-755.7	-687.6

Table S11: Average angles ω_{phenyl} between TCS phenyl rings from production stages of individual AIMD trajectories and their standard deviations.

	$\overline{\omega}_{phenyl}$ [°]	StDev [°]		$\overline{\omega}_{phenyl}$ [°]	StDev [°]
TCS, Traj1	80.8	20.5			
TCS, Traj2	81.8	17.2			
TCS, Traj3	82.2	23.7			
TCS@FAU, Traj1	79.8	13.3	TCS@H-FAU, Traj1	78.8	25.5
TCS@FAU, Traj2	91.8	16.2	TCS@H-FAU, Traj2	86.3	23.4
TCS@FAU, Traj3	90.4	17.5	TCS@H-FAU, Traj3	81.4	18.2
TCS@MOR, Traj1	72.8	25.5	TCS@H-MOR, Traj1	16.8	16.5
TCS@MOR, Traj2	68.8	18.8	TCS@H-MOR, Traj2	21.4	13.5
TCS@MOR, Traj3	68.1	16.7	TCS@H-MOR, Traj3	29.0	12.0
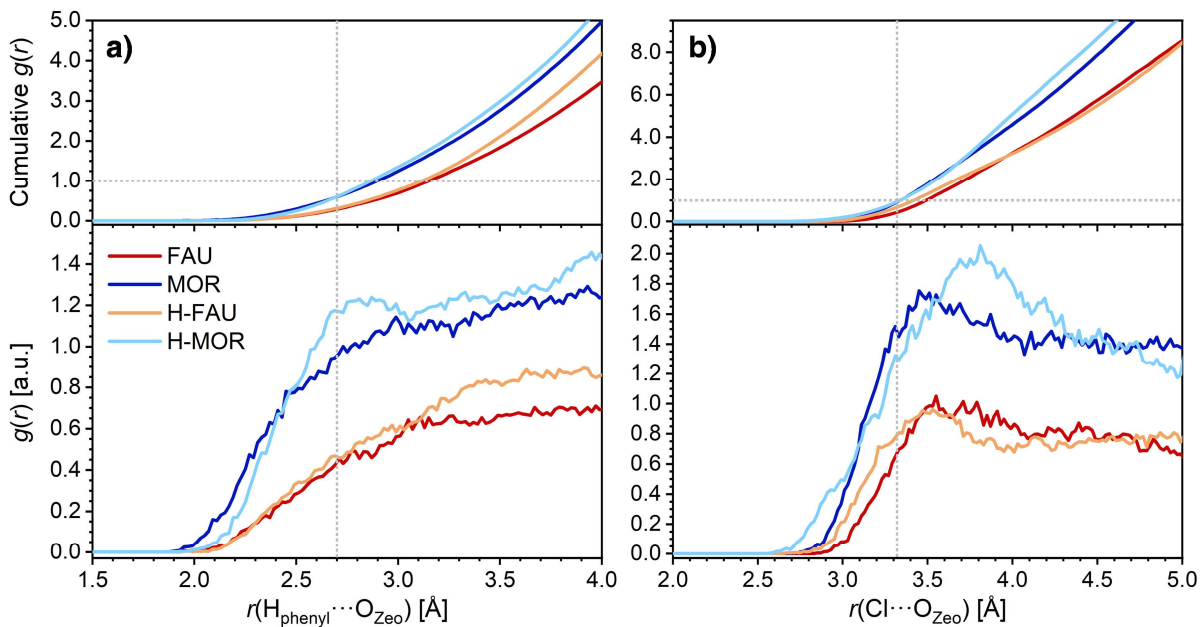
Figure S4: RDFs obtained from AIMD simulations. **(a)** H$_{phenyl}$···O$_{Zeo}$ contacts, **(b)** Cl···O$_{Zeo}$ contacts. The sums of the van der Waals radii are indicated as thin grey lines. Top panels show the cumulative RDFs.
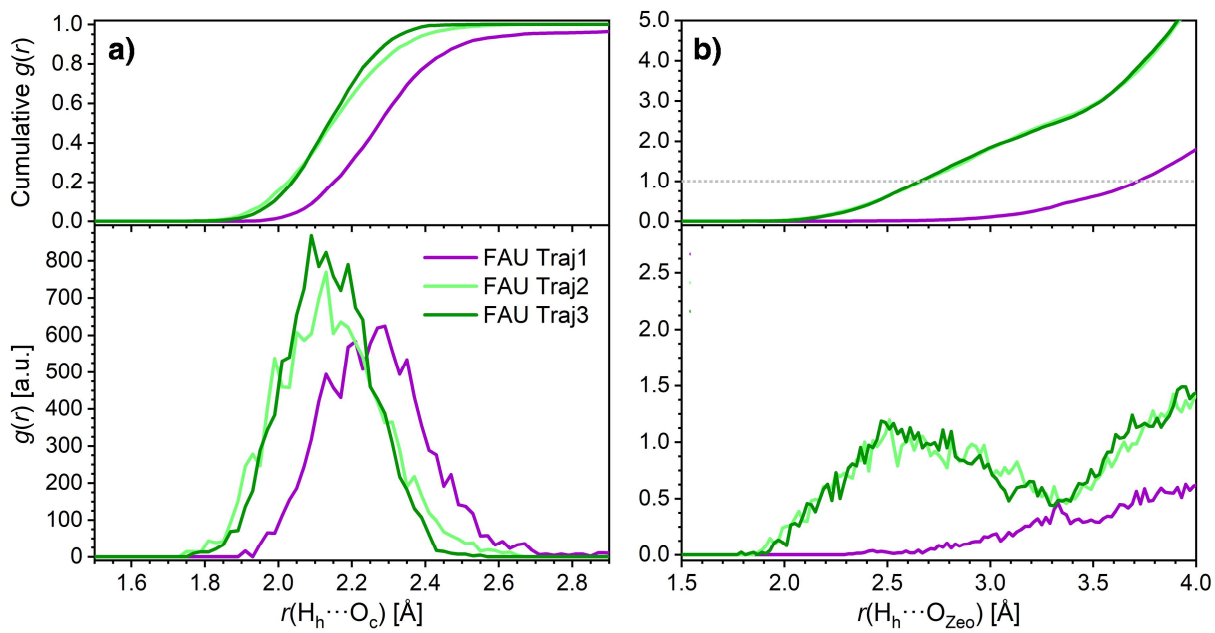
Figure S5: RDFs obtained from AIMD simulations for individual TCS@FAU trajectories. **(a)** Intramolecular hydrogen bonds of TCS, **(b)** $H_h \cdots O_{Zeo}$ hydrogen bonds. Top panels show the cumulative RDFs. Averages shown in the main paper were computed from Traj2 and Traj3.


| TCS@FAU | AIMD, Traj1 | AIMD, Traj2 | AIMD, Traj3 |
| Config3,optimized | last frame | last frame | last frame |
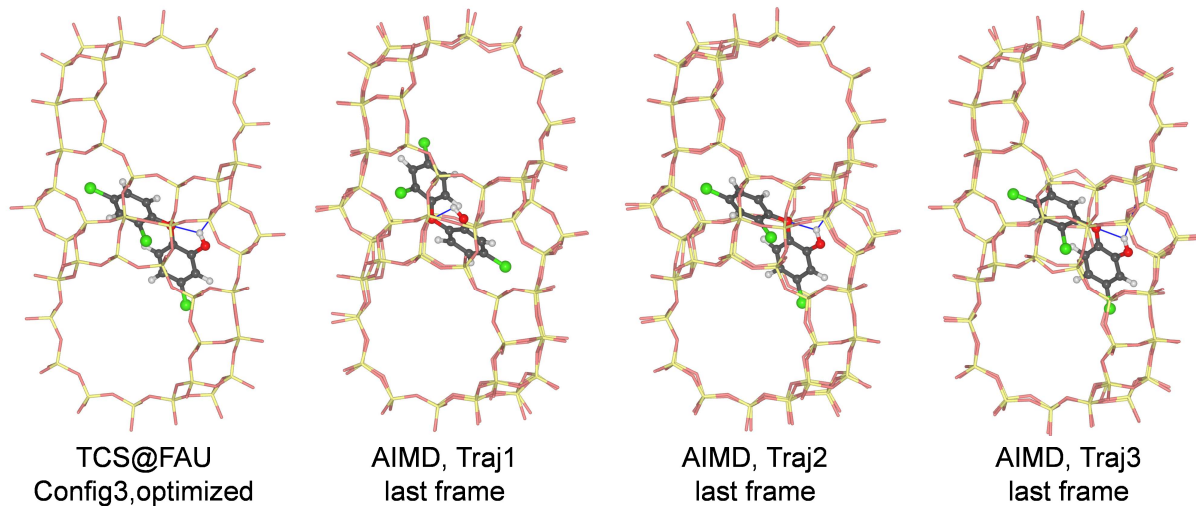
Figure S6: TCS@FAU adsorption configurations: Lowest-energy DFT-optimized structure (left panel) and last frames from three independent AIMD trajectories (remaining panels).
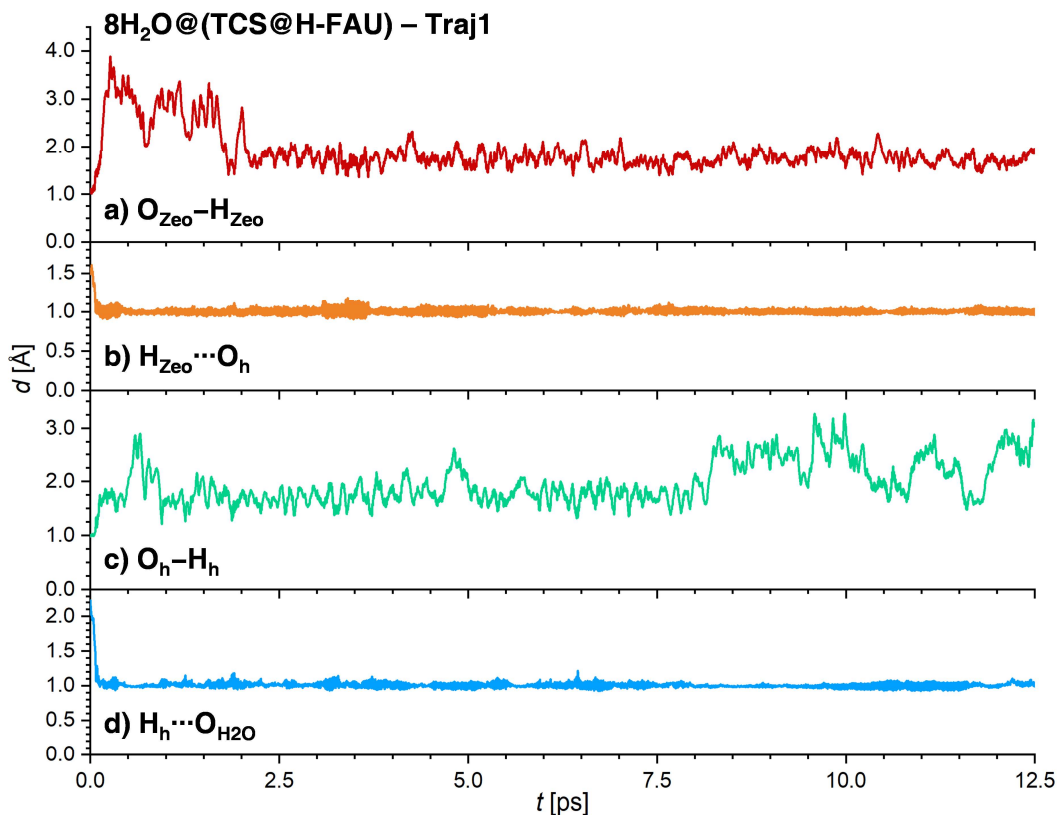
Figure S7: Evolution of selected interatomic distances for the entire AIMD trajectory Traj1 computed for 8H$_2$O@(TCS@H-FAU)
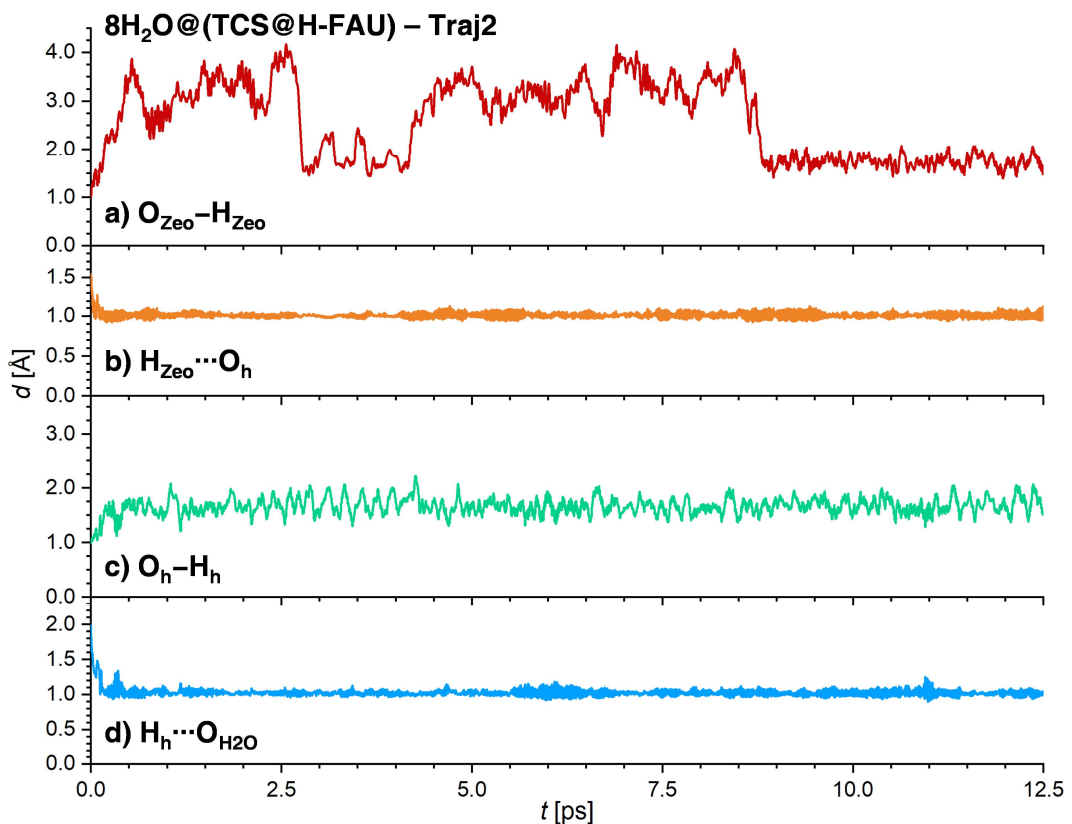
Figure S8: Evolution of selected interatomic distances for the entire AIMD trajectory Traj2 computed for 8H$_2$O@(TCS@H-FAU)
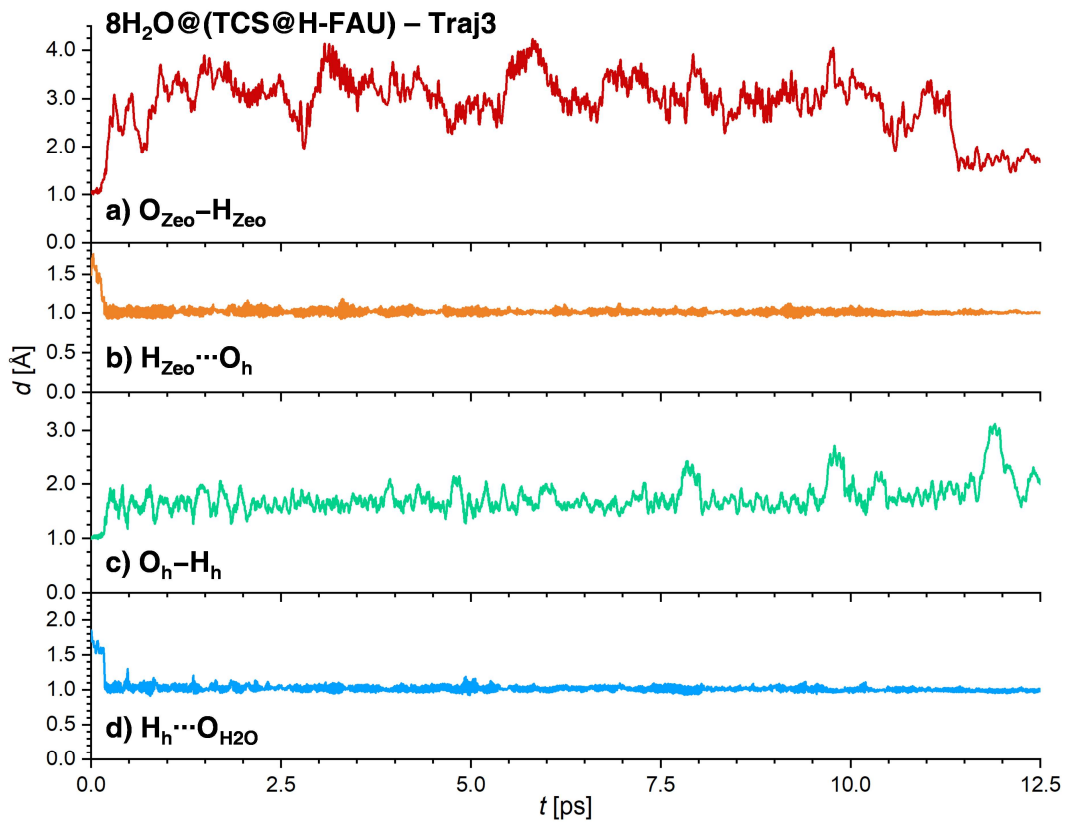
**Figure S9:** Evolution of selected interatomic distances for the entire AIMD trajectory Traj3 computed for 8H$_2$O@(TCS@H-FAU)
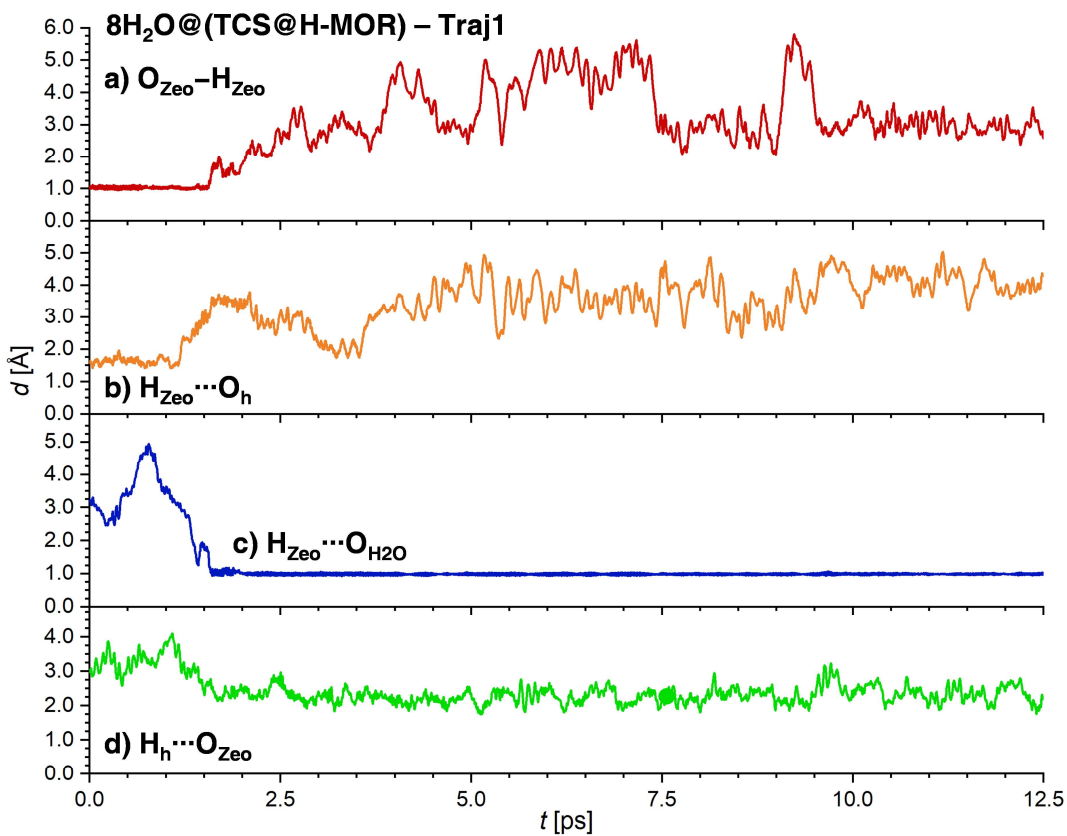
Figure S10: Evolution of selected interatomic distances for the entire AIMD trajectory Traj1 computed for 8H$_2$O@(TCS@H-MOR)
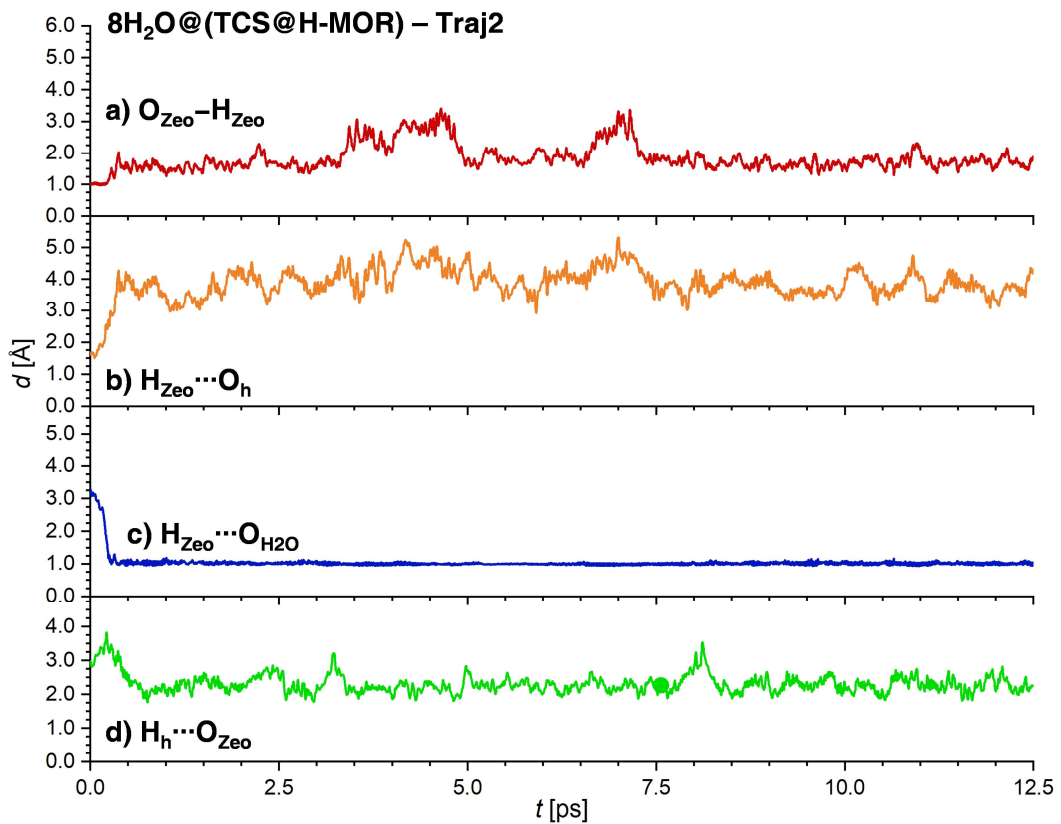
Figure S11: Evolution of selected interatomic distances for the entire AIMD trajectory Traj2 computed for 8H$_2$O@(TCS@H-MOR)
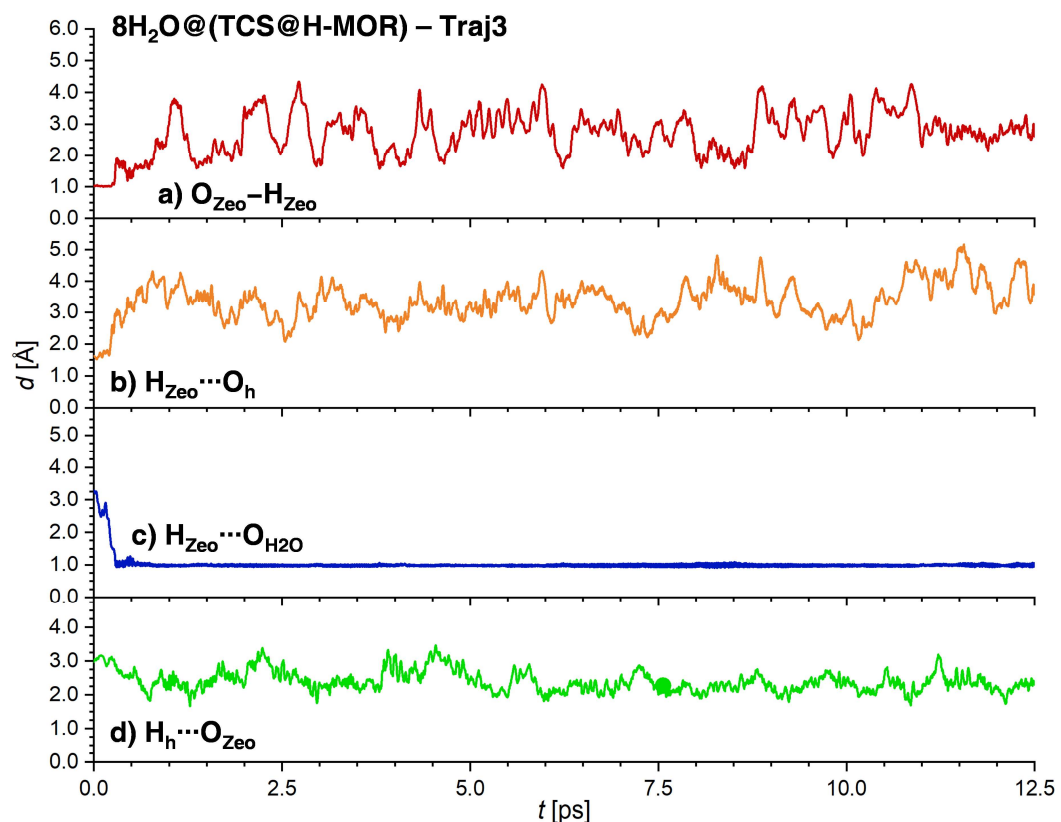
**Figure S12:** Evolution of selected interatomic distances for the entire AIMD trajectory Traj3 computed for 8H$_2$O@(TCS@H-MOR)

References

1   H. Sun, S. J. Mumby, J. R. Maple and A. T. Hagler, An ab Initio CFF93 All-Atom Force Field for Polycarbonates, *J. Am. Chem. Soc.*, 1994, **116**, 2978–2987.

2   M. Waldman and A. T. Hagler, New combining rules for rare gas van der Waals parameters, *J. Comput. Chem.*, 1993, **14**, 1077–1084.

3   A. I. Ramos, S. S. Braga and F. A. Almeida Paz, Triclosan, *Acta Crystallogr. Sect. C Cryst. Struct. Commun.*, 2009, **65**, o404–o405.

4   R. Bialek, W. M. Meier, M. Davis and M. J. Annen, The synthesis and structure of SSZ-24, the silica analog of $AlPO_4$-5, *Zeolites*, 1991, **11**, 438–442.

5   P. A. Barrett, M. A. Camblor, A. Corma, R. H. Jones and L. A. Villaescusa, Structure of ITQ-4, a New Pure Silica Polymorph Containing Large Pores and a Large Void Volume, *Chem. Mater.*, 1997, **9**, 1713–1715.

6   R. Fantini, R. Arletti, S. Quartieri, M. Fabbiani, S. Morandi, G. Martra, F. Di Renzo and G. Vezzalini, Thermal behavior of high silica mordenite, *Microporous Mesoporous Mater.*, 2020, **294**, 109882.

7   J. B. Higgins, R. B. LaPierre, J. L. Schlenker, A. C. Rohrman, J. D. Wood, G. T. Kerr and W. J. Rohrbaugh, The framework topology of zeolite beta, *Zeolites*, 1988, **8**, 446–452.

8   J. A. Hriljac, M. M. Eddy, A. K. Cheetham, J. A. Donohue and G. J. Ray, Powder Neutron Diffraction and ^{29}Si MAS NMR Studies of Siliceous Zeolite-Y, *J. Solid State Chem.*, 1993, **106**, 66–72.

9   P. Wagner, M. Yoshikawa, M. Lovallo, K. Tsuji, M. Taspatsis and M. E. Davis, CIT-5: a high-silica zeolite with 14-ring pores, *Chem. Commun.*, 1997, 2179–2180.